



An allosteric redox switch involved in oxygen protection in a CO₂ reductase

Ana Rita Oliveira, Cristiano Mota, Guilherme Vilela-Alves, Rita Rebelo Manuel, Neide Pedrosa, Vincent Fourmond, Kateryna Klymanska, Christophe Léger, Bruno Guigliarelli, Maria João Romão, et al.

► To cite this version:

Ana Rita Oliveira, Cristiano Mota, Guilherme Vilela-Alves, Rita Rebelo Manuel, Neide Pedrosa, et al.. An allosteric redox switch involved in oxygen protection in a CO₂ reductase. *Nature Chemical Biology*, 2024, 20 (1), pp.111-119. 10.1038/s41589-023-01484-2 . hal-04383526

HAL Id: hal-04383526

<https://hal.science/hal-04383526>

Submitted on 9 Jan 2024

HAL is a multi-disciplinary open access archive for the deposit and dissemination of scientific research documents, whether they are published or not. The documents may come from teaching and research institutions in France or abroad, or from public or private research centers.

L'archive ouverte pluridisciplinaire **HAL**, est destinée au dépôt et à la diffusion de documents scientifiques de niveau recherche, publiés ou non, émanant des établissements d'enseignement et de recherche français ou étrangers, des laboratoires publics ou privés.

An allosteric redox switch involved in oxygen protection in a CO₂ reductase

Ana Rita Oliveira^{1,‡}, Cristiano Mota^{2,3,‡}, Guilherme Vilela-Alves^{2,3}, Rita Rebelo Manuel¹, Neide Pedrosa¹, Vincent Fourmond⁴, Kateryna Klymanska^{2,3}, Christophe Léger⁴, Bruno Guigliarelli⁴, Maria João Romão^{2,3*} and Inês A. Cardoso Pereira^{1*}

¹Instituto de Tecnologia Química e Biológica, Universidade Nova de Lisboa, Av. da República, 2780-157 Oeiras, Portugal

²Associate Laboratory i4HB – Institute for Health and Bioeconomy, NOVA School of Science and Technology, Universidade NOVA de Lisboa, 2829-516 Caparica, Portugal

³UCIBIO, Applied Molecular Biosciences Unit, Department of Chemistry, NOVA School of Science and Technology, Universidade NOVA de Lisboa, 2829-516 Caparica, Portugal

⁴Aix Marseille Univ, CNRS, BIP, Laboratoire de Bioénergétique et Ingénierie des Protéines, Marseille 13402, France

*Corresponding author: ipereira@itqb.unl.pt

mjr@fct.unl.pt

‡ contributed equally

Abstract

Metal-dependent formate dehydrogenases reduce CO₂ with high efficiency and selectivity, but are usually very oxygen sensitive. An exception is *Desulfovibrio vulgaris* W/Sec-FdhAB, which can be handled aerobically, but the basis for this oxygen tolerance was unknown. Here we show that FdhAB activity is controlled by a redox switch based on an allosteric disulfide bond. When this bond is closed, the enzyme is in an oxygen-tolerant resting state presenting almost no catalytic activity and very low formate affinity. Opening this bond triggers large conformational changes that propagate to the active site, resulting in high activity and high formate affinity, but also higher oxygen sensitivity. We present the structure of activated FdhAB and show that activity loss is associated with partial loss of the metal sulfido ligand. The redox switch mechanism is reversible *in vivo* and prevents enzyme reduction by physiological formate levels, conferring a fitness advantage during O₂ exposure.

Introduction

The efficient catalytic conversion of CO₂ into chemicals and fuels presents a major challenge due to the intrinsic kinetic and thermodynamic stability of this molecule. Reduction of CO₂ is very energy demanding and requires coupled proton and electron transfer occurring at low redox potentials, which leads to strong competition from the H⁺ reduction reaction^{1–3}. In addition to the high energy requirements, chemical catalysis of CO₂ reduction has low catalytic efficiency and low product selectivity. In contrast, Nature has evolutionary tailored some enzymes to efficiently and selectively

convert CO₂ with high turnovers and without the need for very low potentials. This involves the use of hydrophobic active sites that promote CO₂ binding and activation, the steric control of independent proton and electron transfer and the stabilization of intermediates, towards formation of single products⁴.

One of the simplest and most interesting CO₂ reactions is its reduction to formate. Formate has a high energy content and can be used directly in fuel cells, as a hydrogen storage material or as a precursor for chemical synthesis⁵⁻⁷. Reduction of CO₂ to formate involves the formal transfer of a hydride (two electrons and one proton), and in nature is efficiently performed by metal-dependent formate dehydrogenases (FDHs), which achieve CO₂ reduction at the thermodynamic potential through the spatially separate transfer of two electrons and one proton to selectively produce formate, while fully preventing the hydrogen evolution reaction^{8,9}. Biologically, most FDHs are tailored for formate oxidation, but metal-dependent FDHs performing CO₂ reduction are involved in either the reductive acetyl-CoA pathway, the most energy-efficient pathway of CO₂ fixation¹⁰, or in syntrophic production of formate for interspecies electron transfer^{11,12}. Both metabolisms are present in anaerobic prokaryotes, such as methanogens, acetogens, syntrophic bacteria and sulfate reducers where we can also find the most active FDHs in CO₂ reduction¹³⁻¹⁵. These enzymes contain a Mo or W atom at the active site coordinated by the dithiolene of two metallopterin guanosine dinucleotide (MGD) groups, one labile sulfur ligand, and a protein-ligand (cysteine or selenocysteine (Sec))¹⁶. W-dependent FDHs are particularly active in CO₂ reduction due to the lower redox potential of this metal^{8,14,17,18}, but most are typically very oxygen-sensitive. Among these, the W and Sec FdhAB enzyme from *Desulfovibrio vulgaris* Hildenborough (*D. vulgaris* H) is remarkable because it has high CO₂ reduction activity but can be purified and handled aerobically¹⁴, which is a major advantage for potential applications. This enzyme has a simple composition with only two subunits, the large catalytic subunit containing the deeply buried Sec/bis-MGD/W cofactor and one [4Fe-4S] center, and the small subunit containing three additional [4Fe-4S] centers responsible for electron transfer to and from the active site. *D. vulgaris* H FdhAB (FDH1) is the main FDH expressed by this organism in the presence of W and is the enzyme involved in CO₂ reduction during syntrophic metabolism^{19,20}. It has high affinity and reduction activity for CO₂ and a remarkable robustness, making it an excellent model system that has been extensively explored in different approaches for sustainable CO₂ reduction²¹⁻²⁵. However, the molecular determinants conferring oxygen tolerance to FdhAB were so far unknown.

Here, we report that an allosteric disulfide bond present at the surface of FdhAB is critical to its robustness by acting as a redox switch that converts the enzyme from a resting, O₂-tolerant, but almost inactive state when the disulfide is closed, to the fully active, but more O₂-sensitive one when the disulfide is open. Reduction of this disulfide bond leads to a series of structural changes that propagate towards the catalytic site, revealing a different active conformation and the involvement of previously unidentified residues important for catalysis. In addition, the resting (inactive) state has lower affinity for formate with a K_M more than two orders of magnitude higher than the active state. O₂ resistance requires the keeping of the active site in the oxidised state, and the role of forming the disulfide bridge is to ensure that *in vivo* the enzyme is not reduced by physiological formate levels while the cells are transiently exposed to oxygen.

Results

FdhAB activity requires reductive activation. After aerobic isolation, *D. vulgaris* H FdhAB displays no CO₂ reduction and very low formate oxidation activity (Fig. 1a). Reductive activation with a thiol reducing agent (DTT or TCEP) is required for full activity (Table 1)¹⁴. A requirement for reductive activation has also been reported for other metal-dependent FDHs, even after anaerobic purification^{18,26,27}. Remarkably, the strong reductant sodium dithionite is not capable of activating FdhAB (Fig. 1a), indicating that reduction of the metal or a low redox potential is not sufficient for FdhAB activation.

When anaerobically purified, FdhAB does not require reductive activation by DTT (Fig. 1c and d), being in a form that we will refer to as the active state. In contrast, when FdhAB is aerobically purified less than 40% of the activity is recovered by activation, and the process is poorly reproducible as the protein easily loses activity. We tested whether oxidation of the crude extract before purification had an effect on the activity and stability of the enzyme. We found that when the crude soluble extract was oxidized under air before purification, a much more stable protein was obtained, which was isolated in an (almost) inactive state, which we called the resting state, and which could be fully activated by DTT in a reproducible way (Fig. 1c and d). Notably, in this resting state the enzyme displays no CO₂ reduction activity and the K_M for formate is very high, 2.5 ± 0.17 mM, two orders of magnitude higher than that of the active enzyme (16.9 ± 2.8 μ M) (Table 1). **The FdhAB C845-C872 bond is a redox switch.** The previous results suggest that reduction of a disulfide bond may be involved in the activation of FdhAB. Inspection of the *D. vulgaris* H FdhAB structure shows the presence of a single disulfide bond on the enzyme surface¹⁴ (Fig. 1b), which is also present in the homologous *Desulfovibrio gigas* enzyme²⁸. In *D. vulgaris* H FdhAB this disulfide bond, between C845 and C872, connects two loops and is present in the oxidized as well as in the formate- and dithionite-reduced crystal structures previously reported^{14,29,30}. No other cysteines are present at the surface, which could form intermolecular disulfide bonds. The C845-C872 disulfide bond is 25 Å away from the W active site, in the opposite direction to the electron transfer pathway, and it is not obvious how it influences enzyme activity. To assess the role of the C845-C872 disulfide bond in reductive activation and its influence on enzyme stability and resistance to O₂, two FdhAB variants were produced: C872A and C845A. These variants present a high activity that is independent of DTT activation (Fig. 1c and 1d), suggesting that without the disulfide bond the enzyme is present in an active conformation. Notably, the C872A variant displays even higher activity than the WT FdhAB (Table 1, Fig. 1c and 1d), whereas the C845A mutation has an overall negative effect on the activity. Aerobic purification of the variants is possible but leads to a decrease in activity, both for formate oxidation and CO₂ reduction, with or without DTT, an effect that is more evident for the C845A variant. This indicates that O₂ sensitivity is not determined only by the disulfide bond. The two variants have similar melting temperatures to the wild type (WT) FdhAB (79 ± 0.1 °C for C845A, 81 ± 0.1 °C for C872A versus 80 ± 0.2 °C for the WT)¹⁴, showing that cleavage of the disulfide bond does not affect the thermostability of the enzyme. In contrast to C872, residue C845 is part of the common core structure of FDH catalytic subunits (Supplementary data 1 and Supplementary Fig. 1), suggesting a possible structural role that may explain the lower activity of variant C845A. Therefore, further experiments were performed only with the C872A variant. This variant presents similar or higher

affinity and activity for formate or CO₂ conversion as the DTT-activated WT enzyme (Table 1, Extended Data Fig. 1), and so is a good proxy for the activated form of the enzyme.

Activated FdhAB presents a strong W^V population. The conformation of the metal active site in FDHs can be probed with great sensitivity using EPR spectroscopy that measures the W^V intermediate state^{13,16,17,31}. The EPR properties of WT FdhAB were recently characterized after reduction with dithionite or formate²⁹. Depending on the reductant, the major species were named W^V_D for dithionite-reduced enzyme ($g = 1.993, 1.909, 1.852$) (Fig. 2a) and W^V_F for formate-reduced enzyme ($g = 1.995, 1.881, 1.852$) (Fig. 2b). These species differ mainly in the g_2 -value while g_1 and g_3 are nearly identical. This difference was interpreted as arising from only a few degrees variation of the SSSS dihedral angles of the W pterin ligands in the two forms. However, a striking observation was the much stronger intensity of the W^V_F signal (~0.2 spins/molecule) obtained after DTT-activation and formate reduction, relative to the intensity of the unactivated dithionite-reduced form, which was not treated with DTT (~0.02 spins/molecule).

EPR analysis of the dithionite or formate reduced C872A variant reveals the presence of W^V_D and W^V_F signals, respectively, both with similar high intensity (Fig. 2c and 2d), in contrast to WT FdhAB. Reduction with formate results in a W^V signal corresponding to 0.18 ± 0.02 spin/molecule (90% W^V_F, 10% W^V_D), and with dithionite in a more mixed signal corresponding to 0.30 ± 0.03 spin/molecule, with about 85% W^V_D and 15% W^V_F (Extended Data Fig. 2). This suggests that the absence of the C845-C872 bond leads to a conformational change that results in a high-intensity W^V EPR signal regardless of reductant used. This is in contrast to the formate-reduced¹⁴ or dithionite-reduced²⁹ forms of the resting WT enzyme with a closed disulfide bond, which presents no or very weak EPR signals. Interestingly, the two different W^V signals can be present in the same sample, showing some heterogeneity in the conformation of the W ligands. The long-range conformational changes at the active site, induced by FdhAB activation (see below), are reminiscent of the remote effects observed in Nitrate reductase A, another member of the Mo/W-enzyme family, where the motion of a distant amino-acid side chain propagates through the H-bond network to the Mo-cofactor and modify its structural surrounding, redox properties and catalytic activity³². Since the only striking difference between the WT and C872A FdhAB is the increase in signal intensity, this firmly suggests that the low intensity W^V signal observed in the dithionite-reduced enzyme (not activated by DTT, disulfide bond closed) is most likely derived from a small fraction of enzyme that has the disulfide bond open, and that the resting, closed state of the enzyme is EPR silent and cannot be reduced to the W^V intermediate state, as previously reported for formate-reduced FdhAB without DTT activation¹⁴.

The crystal structure of C872A FdhAB. The reported structures of *D. vulgaris* H FdhAB (as-isolated aerobically, formate or dithionite reduced^{14,29,30}) all include the C845-C872 disulfide bond. Attempts to obtain a structure with a reduced disulfide bond by incubation or soaking experiments with DTT or TCEP, were unsuccessful. However, the anaerobically purified C872A variant could be crystallized in aerobic and anaerobic conditions, yielding structures C872A_{ox} and C872A_{anox} (the latter complexed with the substrate analogue formamide), which diffracted at 2.3 Å and 1.42 Å, respectively (Supplementary Data 2 and Supplementary Table 1). Both aerobic and anaerobic structures display

identical conformations being superposed with RMSD of 0.26 Å for 971 Cα of FdhA, and of 0.36 Å for 214 Cα of FdhB. In both structures the W site is fully loaded, with B-factors that match neighbouring amino acids, and the position of the MGDs, Sec192 and conserved active site residues H193 and R441 are equivalent. However, the occupancy of the sulfido ligand in the C872A_ox structure is refined at only 56% revealing partial loss of the labile sulfur in aerobic conditions (Extended Data Fig. 3).

Comparing the C872A_anox structure with the as-isolated WT FdhAB structure (PDB ID: 6SDR)¹⁴ reveals that the main conformational changes are in the catalytic subunit (RMSDs of 1.10 Å for 962 Cα of FdhA and 0.34 Å for 214 Cα of FdhB), close to the mutation and in domains III and IV that harbor MGD2. The lack of the disulfide bond induces a long-range conformational rearrangement propagating from the surface down to the active site (Fig. 3), with reorientation of numerous side chains and suggesting the presence of an allosteric mechanism. In the C872A_anox structure, C845 and A872 side chains are far apart, with Cα-845 5.37 Å away from its position when the disulfide bond is present, and Cα-872 3.37 Å away (Fig. 3a). The loss of constraints imposed by the disulfide bond allows increased freedom of the neighbouring amino acids with formation of two new salt bridges (E844...R934 and E867...K564) as well as new hydrogen bonds and hydrophobic interactions. The loop F862-QIEGE-K868 that was not visible in the WT structure, is well defined in the C872A structures, and seems to push the loop S984---P993 towards the active site with the hydrophobic I992 interacting directly with the Sec192 sidechain (Fig. 3b). The new E844...R934 salt bridge at the protein surface induces a series of conformational changes that propagate to the active site, dragging L843 and P842 towards the active site. These changes affect the position of the nearby loop, with a drastic movement of amino acids H410 and W407 that adopt new positions (Fig. 3c). The side chain of Q409 also moves closer to MGD2 (creating a H-bond with the pterin N15) and cause a strong shift in the side chain of M405 (Cε- Cε distance – 5.21 Å), which rotates towards the W active site causing a displacement of Sec192 that adopts a new rotamer (Fig. 3d, 3e). The movement of M405 impacts the W first and second coordination sphere, bringing the methionine Sδ closer to the Se, and MGD S1 (Fig. 3e and Supplementary Table 2). All these modifications induce a drastic rearrangement of the active site when compared with the WT FdhAB structures available (PDB 6SDR, 6SDV and 7Z5O), where the disulfide bond is present (Fig. 3d and e). In the second coordination sphere of W, catalytic R441 shows a slight deviation, but H193 moves away from the active site and presents a third conformation, not previously seen (Extended Data Fig. 4), closer to the R441 side chain and opening the formate channel¹⁴. Also, both MGDs suffer a displacement that is more evident for MGD2 (Fig. 3d). Interestingly, in the C872A_anox structure one formamide molecule is found in the formate channel, hydrogen bonded to R441 and T450, likely mimicking a transit formate molecule (Extended Data Fig. 5).

M405 is a crucial residue in the FdhAB active site. The conspicuous movement of M405 towards the active site upon enzyme activation suggests a key structural role of M405 in the FdhAB active site. This residue is fairly conserved in periplasmic FDHs (62% M, 27% L, 8% V)¹⁴, but is strictly conserved for Mo/W-dependent FDHs having the C845-C872 motif (Supplementary Tables 3 and 4). To understand the role and possible involvement of M405 in catalysis, the M405A variant was created. This variant has virtually no activity when purified aerobically (<1%), showing no increase with DTT, and has 4-6% activity when purified anaerobically (Fig. 1c and d). Notably, the affinity for CO₂ of the M405A

variant is around 40 times lower than WT FdhAB (Table 1), while the affinity for formate is not strongly affected. Also, the optimal pH for CO₂ reduction is shifted to pH 6.0 instead of 7.1 for the WT enzyme (Supplementary Fig. 2), likely due to the strong decrease in CO₂ affinity, such that the CO₂ concentrations at pH 7.1 become non-saturating.

The anaerobically purified M405 variant, with an open disulfide bond, gave a W^V EPR signal with g-values at about 2.003 ± 0.001 , 1.885 ± 0.002 and 1.849 ± 0.002 , close to those of the W^V_F species observed in the C872A variant and in the activated WT FdhAB, with similar spin intensity ($\sim 0.2 \pm 0.03$ spin/molecule) but exhibiting much larger linewidths (Fig. 2c and Extended Data Fig. 2). This broadening likely results from a marked g-strain effect that indicates an increased distribution of conformations of the W-cofactor surroundings, but contribution of unresolved hyperfine interactions cannot be excluded. Both the shape of this signal and its intensity were not affected by a subsequent reduction with dithionite (Extended Data Fig. 6). In contrast, incubation of the variant with formate led to a weaker signal in line with its poor catalytic activity.

The anaerobically purified M405A variant did not crystallize, but the aerobically purified form gave suitable crystals revealing an overall fold similar to WT FdhAB (RMSD 0.41 Å for 955 Cα of FdhA and 0.29 Å for 214 Cα of FdhB), including the C845-C872 region where the disulfide bond is present. Nonetheless, notable changes are observed in the active site and its vicinity, including a pronounced conformational change of the neighbouring Q409 (conserved in FDHs with the double cysteine motif, Supplementary Table 4), which occupies the vacant space left by the mutation (Extended Data Fig. 7). This movement disturbs the active site geometry, which is partially disordered resulting in multiple orientations of the Sec192 sidechain, which exhibits weak electron density and could not be correctly modelled. The B-factors of the active site core are also relatively high, considering the high-resolution of the data, and it was not possible to track the anomalous signal of Se, or model the loop A985---I992. Thus, the substantial decrease in catalytic activity of the M405A variant can be attributed to a disturbed conformation of the coordination sphere of the W active site, caused by the absence of the M405 sidechain. This strongly suggests a key role of M405 in the allosteric mechanism involved in enzyme activation by correct positioning of the Sec192 residue, as well as in the structural integrity/geometry of the active site by stabilizing the W first coordination sphere through nonbonding interactions. These include hypervalent nonbonding S...X (X= O,N,S) interactions, as previously reported for other enzymes with a methionine close to the active site, where such interactions were shown to impact reaction efficacy³³. Indeed, several nonbonding S...X interactions involving M405 and residues close to the active site are present in the oxidized and reduced WT FdhAB structures (Supplementary Table 2). Interestingly, the C872A variant has the largest number of S...X interactions (Supplementary Table 2), since the conformational changes of M405 and Q409 led to new S...X interactions not present in the WT, further supporting the functional role of the conserved M405.

Oxygen tolerance of C872A FdhAB. Aerobic purification of C872A FdhAB leads to reduced activity, but this variant is still quite stable in air, when in the oxidized W^{VI} state (Fig. 4a), as previously reported for the resting WT FdhAB, with a closed disulfide bond¹⁴. However, when reduced by excess formate, the C872A variant is much more rapidly inactivated than the resting form of the enzyme, showing a similar behaviour to the DTT-activated WT protein. Long-term storage in aerobic conditions of the oxidized C872A variant reveals less oxygen tolerance than that of the as-

isolated oxidized WT FdhAB with a closed disulfide bond (Supplementary Fig. 3). These results indicate that two factors influence the stability of the enzyme to O₂: the redox state of the metal and to a less extent the state of the disulfide bond. The former plays a stronger role, with the enzyme being rapidly inactivated when it is in the reduced W^{IV} state, but still much faster when the disulfide bond is open than when it is closed (Fig. 4a). Incubation with DTT of formate-reduced O₂-exposed WT protein does not lead to recovery of activity, confirming that the loss of activity is not due to spontaneous reformation of the disulfide bond with O₂.

Chronoamperometry was used to kinetically characterize the O₂ inactivation process of the formate-reduced protein during active turnover, by measuring the catalytic current in the presence of formate, which is proportional to the enzyme turnover frequency³⁴. Notably, no current was detected for the aerobically purified oxidized WT FdhAB, consistent with the very low to no activity of the resting state with a closed disulfide bond. The rate of inactivation by O₂ was determined by measuring the catalytic formate oxidation current over time after injecting an aliquot of O₂-saturated buffer and analysing the subsequent decrease in activity. The O₂ inactivation rates of aerobically purified but DTT-activated WT FdhAB, anaerobically purified WT FdhAB, and C872A variant revealed no significant differences between the three active enzymes (Fig. 4b and 4c, and Supplementary Data 3). The similar inactivation kinetics indicate that the same active state, corresponding to the conformation with the open disulfide bond, is obtained by reducing the C872-C845 bond with DTT, by isolating the enzyme anaerobically or by preventing the disulfide bond formation in the C872A variant. The inactivation is consistent with a bimolecular irreversible reaction with O₂ and is not reverted by applying a low redox potential (E=-670 mV vs SHE) or when the O₂ concentration decreases, suggesting the requirement of protein factors for activation/inactivation.

The C845-C872 redox switch is reversible *in vivo*. The formation and cleavage of disulfide bonds is usually catalyzed by dedicated protein factors³⁵. To try to assess whether the C845-C872 bond is reversibly formed *in vivo*, we performed experiments with whole cells of *D. vulgaris* over-expressing WT FdhAB. These experiments showed that the FdhAB activity of cells in anaerobic conditions is not dependent on DTT (Fig. 5a), suggesting that the enzyme is in the active state without the C845-C872 bond. Upon O₂ exposure for 7 min, the activity is lost but can be partially recovered by DTT, suggesting that the enzyme was converted to the resting state, with a closed disulfide bond, upon O₂ exposure. Incomplete recovery of the activity is expected due to some oxidative damage to the active site. Switching to bubbling with N₂ for another 10 min led to substantial recovery of the enzyme activity, suggesting conversion of the enzyme to the open active state. Addition of DTT further increased the activity, suggesting that part of the enzyme was still in the resting state. In the control condition, where the cells remained under O₂, no activity was recovered without the addition of DTT. These results support the proposal that the C845-C872 disulfide bond is formed reversibly *in vivo* by dedicated enzymes in response to O₂ exposure and acts as a redox switch to control the catalysis of FdhAB (Fig. 5b). More detailed experiments will be required to fully clarify the process and the proteins involved.

A Blast search of the NCBI Protein database with *D. vulgaris* H FdhA identified 94 FDHs containing the double cysteine motif for this redox switch, in bacteria from the orders Desulfovibrionales, Desulfobacterales,

Desulfunomonadales, Syntrophobacterales and Nitrospirales (Supplementary Table 3). All these enzymes are periplasmic, 92% are Sec-containing FDHs and 70% are heterodimeric FdhAB-like enzymes.

Discussion

The strong oxygen sensitivity of metal-dependent, and particularly W-dependent, FDHs is a major drawback for their catalytic application in the context of CO₂ reduction. Some metal-dependent FDHs present a degree of oxygen tolerance for the formate oxidation reaction, but are characterized by low CO₂ reduction activities, which limits their application^{36–38}. Here we propose a mechanism, present in some metal-dependent FDHs from anaerobic bacteria, allowing partial protection from oxidative inactivation, based on the presence of an allosteric disulfide bond, which needs to be reduced for the enzyme to be active. Disulfide bonds in proteins were classically considered to be involved in stabilizing protein structures or having a functional role as in thiol-disulfide oxidoreductases³⁹. However, allosteric disulfide bonds have come to be recognized as an important post-translational mechanism for controlling protein function through the triggering of conformational changes upon cleavage/formation of this bond³⁵. Such allosteric disulfides have been identified from viruses to mammals, and many are present in extracellular human proteins and are important drug targets³⁵. Recently, a new type of allosteric bond was also described involving a lysine and a cysteine through a nitrogen–oxygen–sulfur (NOS) bridge, which is also widespread in all domains of life^{40,41}. Proteins with allosteric disulfides have been implicated in ligand binding, substrate hydrolysis, proteolysis, or oligomerization, but, to our knowledge, not in oxidoreductases.

By first oxidizing the sulfide-rich crude cell extract, we could isolate FdhAB aerobically in a stable, but almost inactive resting state, which has a closed disulfide bond and withstands O₂ exposure for prolonged periods of time, in the absence of reductant, allowing facile manipulation of the enzyme. This is a major advantage for catalytic CO₂ reduction devices as the enzyme can be easily turned on *in situ* when desired^{21–25}. FdhAB inactivation by O₂ is mainly observed once W is reduced and is much faster when the disulfide bond is open than when it is closed. This suggests that formate and/or O₂ access to the active site is faster when this bond is open. The faster inactivation of the active form, mimicked by the C872A variant, involves the partial loss of the catalytically essential sulfido ligand, as shown in the aerobic C872A structure where it has only 56% occupancy. The sulfido ligand is more quickly displaced in the reduced W^{IV}-SH state and at higher pH⁴², and its loss may be associated with superoxide production by the reduced enzyme upon contact with O₂⁴³.

Besides the absence or very low activity of the FdhAB resting state, its pronounced decrease in formate affinity is of high physiological relevance. Formate concentrations in anoxic environments are usually in the low micromolar range (~20 μM), allowing syntrophic interactions based on formate (and H₂) cycling^{44,45}. Thus, when in the closed resting state, FdhAB is not likely to be reduced by formate *in vivo*, which leaves its active site in the O₂-insensitive W^{VI} state. This suggests that the redox switch mechanism evolved to allow protection of FdhAB against formate-induced reduction during periods of oxidative stress, by lowering formate affinity and preventing enzyme reduction and subsequent inactivation. Thus, the main role of forming the disulfide bond is probably not direct protection against oxygen, but more likely to prevent reduction of the enzyme by physiological formate concentrations to avoid

formation of the reduced O₂-sensitive state. Once anoxic conditions are restored, the C845-C872 bond is opened, triggering structural changes that are crucial to allow CO₂ reduction and that drastically increase the affinity for formate and the catalytic efficiency of its oxidation. These changes were identified through the crystal structures of the C872A variant, which represent the structure of FdhAB in the activated state. These structures reveal the active conformation of the enzyme as well as the sequence of conformational changes involved in the redox switch mechanism to originate the catalytically competent state. These changes are especially relevant close to the active site, where M405 seems to have a prominent role in positioning Sec192 and maintaining the necessary active site geometry for efficient catalysis. Interestingly, a close interaction between L410 and C196, equivalent to M405 and U192 in FdhAB, was also identified in the *E. coli* Fdh-N active site using QM/MM geometry optimizations⁴⁶.

The double cysteine motif is conserved among FDHs from other anaerobes, namely many sulfate-reducing organisms that live in environments transiently exposed to O₂^{47–50}. The possibility of forming this disulfide bond in response to the redox conditions is likely an evolutionary adaptation^{51,52} that constitutes a major advantage *in vivo* by protecting the enzyme and allowing a fast transition to the active state, without the need for *de novo* protein synthesis. In fact, sulfate reducing bacteria are notorious for having several mechanisms to detoxify O₂^{53–55}, and also for having evolved ingenious systems for protecting sensitive enzymes from oxidative stress, based on formation of resting states that are resistant to damage but can be quickly reactivated when O₂ is removed. Examples are PFOR (pyruvate-ferredoxin oxidoreductase), which presents a protein extension that can protect an O₂-sensitive iron-sulfur cluster and is locked in this position by formation of a disulfide bond⁵⁶, and the [FeFe] and [NiFeSe] hydrogenases where a transient sulfur ligand at the active site protects them from oxidative damage^{57–59}. An alternative strategy is present in the CO dehydrogenase where the typical [4Fe-4S] cluster close to the surface is substituted by an oxygen-resistant [2Fe-2S] cluster⁶⁰.

In conclusion, we identified a redox switch mechanism present in the *D. vulgaris* H FdhAB that forms the basis for its remarkable oxygen tolerance and allows its successful application in light or electricity-driven CO₂ reduction systems^{21–25}. This mechanism is based on an allosteric disulfide bond that controls enzyme activity and formate affinity, and physiologically prevents enzyme reduction and subsequent O₂ sensitivity. The redox switch is present in other FDHs from anaerobic bacteria, most typically in highly active as well as highly O₂-sensitive W- and Sec-containing heterodimeric FDHs and is likely a key evolutionary advantage in the aerotolerance of these organisms.

Acknowledgments

This work was financially supported by Fundação para a Ciência e Tecnologia (FCT, Portugal) through fellowships SFRH/BD/116515/2016 (A.R.O.) and DFA/BD/7897/2020 (R.R.M.), COVID/BD/151766/2021 (A.R.O.), grant PTDC/BII-BBF/2050/2020 (I.A.C.P. and M.J.R.), and R&D units MOSTMICRO-ITQB (UIDB/04612/2020 and UIDP/04612/2020) (I.A.C.P.) and UCIBIO (UIDP/04378/2020 and UIDB/04378/2020) (M.J.R.), and Associated Laboratories LS4FUTURE (LA/P/0087/2020) (I.A.C.P.) and i4HB (LA/P/0140/2020) (M.J.R.). European Union's Horizon 2020 research and innovation program (Grant agreement no. 810856) is also acknowledged (I.A.C.P.). This work was

also funded by the French national research agency (ANR – MOLYERE project, grant number 16-CE-29-0010-01) (B.G.), and supported by the computing facilities of the CRCMM, Centre Régional de Compétences en Modélisation Moléculaire de Marseille. We thank the excellent technical assistance of João Carita from ITQB NOVA on microbial cell growth. We are also grateful to the EPR-MRS facilities of the Aix-Marseille University EPR centre and acknowledge the support of the European research infrastructure MOSBRI (Grant Agreement N° 101004806) (B.G.) and the French research infrastructure INFRANALYTICS (FR2054) (B.G.). We also acknowledge the European Synchrotron Radiation Facility and ALBA Synchrotron for provision of synchrotron radiation facilities, and we would like to thank the staff of the ESRF and EMBL Grenoble and ALBA for assistance and support in using beamlines ID23-1, ID30A-3, ID30B and XALOC.

Author Contributions

I.A.C.P. and A.R.O. conceived and designed biochemical experiments and sequence analysis. A.R.O. performed molecular biology experiments, protein purification, biochemical characterization, enzymatic assays, sequence analysis, EPR and electrochemical studies of WT, C845A and C872A variants and figure preparation. R. R. M. produced and characterized the M405A variant and contributed to CO₂ reduction assays and figure preparation. C.M., M.J.R. and G.V.A. designed the crystallography experiments and analysed the crystal structures. C.M. and G.V.A. performed TSA assays, crystallized the proteins, solved and refined all structures. G.V.A. prepared all figures with crystal structures. K.K. helped with crystallization assays and first stages of refinement of the 8CM4 and 8CM5 structures. V.F. and C.L. designed electrochemical experiments, performed by V.F. and A.R.O.. B.G. designed and analyzed EPR experiments, performed by B.G. and A.R.O.. I.A.C.P., R.R.M. and N.P. designed in vivo experiments, performed by N. P. and R.R.M.. I.A.C.P. and M.J.R. supervised and funded the project. A.R.O., I.A.C.P., M.J.R., C.M., G.V.A., wrote the manuscript with inputs from co-authors V.F., C.L. and B.G. All authors approved the final version of the manuscript.

Competing interests

The authors declare no competing interests.

347

348 **Table 1 | Kinetic parameters of FdhAB WT, C872A, and M405A variants^a**

Condition	DTT in assay		Formate			CO ₂			Ref
			K_M^a (μM)	Turnover (s^{-1})	k_{cat}/K_M ($\text{s}^{-1}\text{mM}^{-1}$)	K_M^a (μM)	Turnover (s^{-1})	k_{cat}/K_M ($\text{s}^{-1}\text{mM}^{-1}$)	
Aerobic	+	WT	16.9 ± 2.8	$1,310 \pm 50$	77,515	324 ± 54	344 ± 41	1,090	14
Aerobic	-		2560 ± 168	94 ± 10	36	-	-	-	this work
Anaerobic	-	C872A	33.7 ± 4.2	$1,485 \pm 95$	44,065	173 ± 16	368 ± 22	2,140	this work
Anaerobic	-	M405A	17.9 ± 1.7	82.4 ± 1.8	4,603	$12,253 \pm 1,942$	43 ± 3	3.5	this work

349 ^aKinetic data were obtained in 50 mM KPi buffer pH 7.6, 2 mM benzyl viologen for formate oxidation, and 100 mM KPi
350 buffer pH 7.1, 0.1 mM reduced methyl-viologen for CO₂ reduction. For determination of the affinity constants, formate
351 concentrations ranging from 0.5 μM to 20 mM and CO₂ concentrations from 18 μM to 5.6 mM (WT and C872A) and
352 312 μM to 23 mM (M405A) were used. CO₂ affinity of M405A was evaluated at pH 6. The kinetic parameters (derived
353 from data in Extended Data Figure 1) were calculated using GraphPad Prism 9 and the Michaelis-Menten equation.
354 Values represent the mean of at least n=3 independent experiments \pm s.d..
355

Figure Legends

Figure 1: Enzymatic activity of FdhAB and variants. **a.** Formate oxidation activity (green), and CO₂ reduction activity (blue) of WT FdhAB as-isolated and pre-treated with 15 mM dithionite prior to activity measurements, evaluated with (+) and without (-) pre-incubation with DTT. 100% of activity calculated with the standard assay (as-isolated enzyme pre-incubated with DTT). Data are based on n=2 independent experiments. Results are plotted individually as dots, and the bars represent the mean. **b.** Representation of WT FdhAB structure highlighting the redox centers and the position of the C845-C872 disulfide bond (distance in Å). **c.** Formate oxidation turnover rates of WT FdhAB (green), C845A (grey), C872A (purple) and M405A (yellow) variants, aerobically and anaerobically purified. **d.** CO₂ reduction turnover numbers of WT FdhAB (blue), C845A (grey), C872A (purple) and M405A (yellow) variants, aerobically and anaerobically purified. Data are based on at least n=3 independent experiments. Results are plotted individually as dots, and the bars represent the mean.

Figure 2: EPR spectra of W^V species in WT FdhAB enzyme (black traces), C872A (blue traces) and M405A (magenta trace) variants. Experimental spectrum of a) resting WT sample poised at -468 mV by reduction with dithionite; b) DTT activated WT sample poised at -395 mV by reduction with formate; c) C872A sample poised at -443 mV by reduction with formate; d) C872A sample poised at -469 mV by reduction with dithionite; e) M405A reduced by dithionite. EPR conditions: temperature 80 K; microwave power 40 mW at 9.479 GHz; modulation amplitude 1 mT at 100 kHz.

Figure 3: Structural changes induced by the allosteric cleavage of the C845-C872 bond. Superposition of FdhAB WT (grey) and C872A_{anox} structures (blue). **a)** Close-up view of the C872A mutation region. **b)** F862---K868 and S984---P993 loops. Loop F862---K868 is defined in the structure of C872A_{anox} and is displacing loop S984---P993. I992 is shown as sticks and the distances between I992 Cδ (in C872A_{anox}) and U192 Cα, in both structures, are indicated. **c)** Conformational changes induced by the lack of the disulfide bond. Residues whose conformations are altered are shown as sticks. Black arrows indicate the allosteric mechanism linking the disulfide bond and the active site. **d)** View of the active site including U192, M405 and Q409. **e)** Close-up view of W active site and M405/U192 movement.

Figure 4: Effect of oxygen on catalysis by WT FdhAB and C872A variant. **a.** Effect of O₂ exposure on formate oxidation activity of as-isolated WT FdhAB (grey symbols)¹⁴, WT FdhAB pre-activated with DTT (green symbols), and C872A variant (blue symbols), incubated aerobically at room temperature in buffer A (open symbols) and buffer A plus 20 mM formate (full symbols). The as-isolated WT FdhAB is treated with DTT only prior to activity measurement. Data are presented as mean values ± s.d. (n = 2 or 3 assay technical replicates). **b.** Effect of O₂ (introduction marked by blue arrow) on formate oxidation current of the active forms of FdhAB: DTT-activated WT FdhAB (green line); anaerobically purified WT FdhAB (grey line); C872A variant (dashed blue line). **c.** Rate of O₂ inactivation calculated according to equation 3 (Supplementary Data 3), from the mean of n=3 independent experiments ± s.d.. Experimental conditions: [O₂] = 30 μM, t = 60 s, 1 mM formate, E = 0.130 V, pH 7, electrode rotation rate = 4000 rpm. Differences are not significant (ns, p>0.05) as estimated using GraphPad prism 7, one-way ANOVA, and Tukey's multiple comparisons test.

Figure 5: Reversibility of the FdhAB redox switch. **a)** Formate oxidation activity of *D. vulgaris* H cells expressing recombinant WT FdhAB, without (green) and with (blue) DTT activation, at time zero (T0), after exposure to 7 min O₂ (T7-O₂), and after further 10 min N₂ (T17-N₂) or continued 17 min O₂ (T17-O₂). All data are based on at least n=3 independent experiments. Results are plotted individually as dots, and the bars represent the mean. The expected status of the C845-C872 disulfide bond is represented. **b)** Scheme of the physiological FdhAB cycle. Upon aerobic treatment of the crude extract and isolation the enzyme is in a resting state with a closed disulfide bond, thus preventing reduction by physiological concentrations of formate. Upon cleavage of the C845-C872 bond the enzyme is activated and can enter the catalytic cycle (grey box). The reduced W^{IV} state is very sensitive to O₂-induced inactivation.

References

1. Dalle, K. E., Warnan, J., Leung, J. J., Reuillard, B., Karmel, I. S. & Reisner, E. Electro- and Solar-Driven Fuel Synthesis with First Row Transition Metal Complexes. (2019). doi:10.1021/acs.chemrev.8b00392
2. Wang, G., Chen, J., Ding, Y., Cai, P., Yi, L., Li, Y., Tu, C., Hou, Y., Wen, Zh. & Dai, L. Electrocatalysis for CO₂ conversion: from fundamentals to value-added products. *Chem. Soc. Rev.* **50**, 4993–5061 (2021).
3. Zhang, S., Fan, Q., Xia, R. & Meyer, T. J. CO₂ Reduction : From Homogeneous to Heterogeneous Electrocatalysis. *Acc Chem Res* **53**, 2–11 (2019).
4. Shi, J., Jiang, Y., Jiang, Z., Wang, X., Wang, X., Zhang, S., Han, P. & Yang, C. Enzymatic conversion of carbon dioxide. *Chem. Soc. Rev.* **44**, 5981–6000 (2015).
5. Yishai, O., Lindner, S. N., Gonzalez de la Cruz, J., Tenenboim, H. & Bar-Even, A. The formate bio-economy. *Curr Opin Chem Biol* **35**, 1–9 (2016).
6. Mellmann, D., Sponholz, P., Junge, H. & Beller, M. Formic acid as a hydrogen storage material – development of homogeneous catalysts for selective hydrogen release. *Chem. Soc. Rev.* (2016). doi:10.1039/C5CS00618J
7. Bulushev, D. & Ross, J. R. H. Towards Sustainable Production of Formic Acid from Biomass for Getting Hydrogen and Fuels. *ChemSusChemus* (2018). doi:10.1002/cssc.201702075
8. Reda, T., Plugge, C. M., Abram, N. J. & Hirst, J. Reversible interconversion of carbon dioxide and formate by an electroactive enzyme. *Proc Natl Acad Sci U S A* **105**, 10654–10658 (2008).
9. Stripp, S. T., Duffus, B. R., Fourmond, V., Léger, C., Leimkühler, S., Hirota, S., Hu, Y., Jasniewski, A., Ogata, H. & Ribbe, M. W. Second and Outer Coordination Sphere Effects in Nitrogenase, Hydrogenase, Formate Dehydrogenase, and CO Dehydrogenase. *Chem Rev* **122**, 11900–11973 Preprint at <https://doi.org/10.1021/acs.chemrev.1c00914> (2022)
10. Schuchmann, K. & Müller, V. Autotrophy at the thermodynamic limit of life : a model for energy conservation in acetogenic bacteria. *Nature Publishing Group* (2014). doi:10.1038/nrmicro3365
11. Plugge, C. M., Zhang, W., Scholten, J. C. M. & Stams, A. J. M. Metabolic flexibility of sulfate-reducing bacteria. **2**, 1–8 (2011).
12. Sieber, J. R., Mcinerney, M. J. & Gunsalus, R. P. Genomic Insights into Syntrophy : The Paradigm for Anaerobic Metabolic Cooperation. *Annu Rev Microbiol* **66**, 429–452 (2012).
13. Niks, D. & Hille, R. Molybdenum- and tungsten-containing formate dehydrogenases and formylmethanofuran dehydrogenases: Structure, mechanism, and cofactor insertion. *Protein Science* **28**, 111–122 (2019).
14. Oliveira, A. R., Mota, C., Mourato, C., Domingos, R. M., Santos, M. F. A. A., Gesto, D., Guigliarelli, B., Santos-Silva, T., Romão, M. J. & Cardoso Pereira, I. A. Toward the Mechanistic Understanding of Enzymatic CO₂ Reduction. *ACS Catal* **10**, 3844–3856 (2020).

15. Dietrich, H. M., Righetto, R. D., Kumar, A., Wietrzynski, W., Trischler, R., Schuller, S. K., Wagner, J., Schwarz, F. M., Engel, B. D., Müller, V. & Schuller, J. M. Membrane-anchored HDCR nanowires drive hydrogen-powered CO₂ fixation. *Nature* **607**, 823–830 (2022).
16. Grimaldi, S., Schoepp-Cothenet, B., Ceccaldi, P., Guigliarelli, B. & Magalon, A. The prokaryotic Mo/W-bisPGD enzymes family: A catalytic workhorse in bioenergetic. *Biochim Biophys Acta Bioenerg* **1827**, 1048–1085 (2013).
17. Hille, R. Molybdenum and tungsten in biology. *Trends Biochem Sci* **27**, 360–367 (2002).
18. Schwarz, F. M., Schuchmann, K. & Müller, V. Hydrogenation of CO₂ at ambient pressure catalyzed by a highly active thermostable biocatalyst. *Biotechnol Biofuels* **11**, 237 (2018).
19. da Silva, S. M., Pimentel, C., Valente, F. M. A. A., Rodrigues-Pousada, C. & Pereira, I. A. C. C. Tungsten and molybdenum regulation of formate dehydrogenase expression in *Desulfovibrio vulgaris* Hildenborough. *J Bacteriol* **193**, 2909–2916 (2011).
20. da Silva, S. M., Voordouw, J., Leitão, C., Martins, M., Voordouw, G. & Pereira, I. A. C. Function of formate dehydrogenases in *Desulfovibrio vulgaris* Hildenborough energy metabolism. *Microbiology (N Y)* **159**, 1760–1769 (2013).
21. Miller, M., Robinson, W. E., Oliveira, A. R., Heidary, N., Kornienko, N., Warnan, J., Pereira, I. A. C. & Reisner, E. Interfacing Formate Dehydrogenase with Metal Oxides for the Reversible Electrocatalysis and Solar-Driven Reduction of Carbon Dioxide. *Angewandte Chemie International Edition* **58**, 4601–4605 (2019).
22. Edwardes Moore, E., Andrei, V., Oliveira, A. R., Coito, A. M., Pereira, I. A. C. & Reisner, E. A Semi-artificial Photoelectrochemical Tandem Leaf with a CO₂-to-Formate Efficiency Approaching 1 %. *Angewandte Chemie International Edition* **60**, 26303–26307 (2021).
23. Szczesny, J., Ruff, A., Oliveira, A. R., Pita, M., Pereira, I. A. C., De Lacey, A. L. & Schuhmann, W. Electroenzymatic CO₂ Fixation Using Redox Polymer/Enzyme-Modified Gas Diffusion Electrodes. *ACS Energy Lett* **5**, 321–327 (2020).
24. Alvarez-Malmagro, J., Oliveira, A. R., Gutiérrez-Sánchez, C., Villajos, B., Pereira, I. A. C., Vélez, M., Pita, M. & De Lacey, A. L. Bioelectrocatalytic Activity of W-Formate Dehydrogenase Covalently Immobilized on Functionalized Gold and Graphite Electrodes. *ACS Appl Mater Interfaces* **13**, 11891–11900 (2021).
25. Antón-García, D., Edwardes Moore, E., Bajada, M. A., Eisenschmidt, A., Oliveira, A. R., Pereira, I. A. C., Warnan, J. & Reisner, E. Photoelectrochemical hybrid cell for unbiased CO₂ reduction coupled to alcohol oxidation. *Nature Synthesis* **1**, 77–86 (2022).
26. De Bok, F. A. M. M., Hagedoorn, P. L., Silva, P. J., Hagen, W. R., Schiltz, E., Fritsche, K. & Stams, A. J. M. M. Two W-containing formate dehydrogenases (CO₂-reductases) involved in syntrophic propionate oxidation by *Syntrophobacter fumaroxidans*. *Eur J Biochem* **270**, 2476–2485 (2003).
27. Schuchmann, K. & Müller, V. Direct and Reversible Hydrogenation of CO₂ to Formate by a Bacterial Carbon Dioxide Reductase. *Science (1979)* **342**, 1382–1385 (2013).

28. Raaijmakers, H., Macieira, S., Dias, J. M., Teixeira, S., Bursakov, S., Huber, R., Moura, J. J. G., Moura, I. & Romão, M. J. Gene Sequence and the 1.8 Å Crystal Structure of the Tungsten-Containing Formate Dehydrogenase from *Desulfovibrio gigas*. *Structure* **10**, 1261–1272 (2002).
29. Oliveira, A. R., Mota, C., Klymanska, K., Biaso, F., Romão, M. J., Guigliarelli, B. & Pereira, I. C. Spectroscopic and Structural Characterization of Reduced *Desulfovibrio vulgaris* Hildenborough W-FdhAB Reveals Stable Metal Coordination during Catalysis. *ACS Chem Biol* 1–23 (2022). doi:10.1021/acschembio.2c00336
30. Vilela-Alves, G., Manuel, R. R., Oliveira, A. R., Pereira, I. C., Romão, M. J. & Mota, C. Tracking W-Formate Dehydrogenase Structural Changes During Catalysis and Enzyme Reoxidation. *Int J Mol Sci* **24**, (2023).
31. Grimaldi, S., Biaso, F., Burlat, B. & Guigliarelli, B. in *Molybdenum and Tungsten Enzymes: Spectroscopic and Theoretical Investigations* (eds. Hille, R., Schulzke, C. & Kirk, M. L.) 68–120 (The Royal Society of Chemistry, 2016). doi:doi.org/10.1039/9781782628842-00068
32. Al-Attar, S., Rendon, J., Sidore, M., Duneau, J.-P., Seduk, F., Biaso, F., Grimaldi, S., Guigliarelli, B. & Magalon, A. Gating of Substrate Access and Long-Range Proton Transfer in *Escherichia coli* Nitrate Reductase A: The Essential Role of a Remote Glutamate Residue. *ACS Catal* **11**, 14303–14318 (2021).
33. Iwaoka, M. & Isozumi, N. Hypervalent Nonbonded Interactions of a Divalent Sulfur Atom. Implications in Protein Architecture and the Functions. *Molecules* **2**, 7266–7283 (2012).
34. Léger, C. & Bertrand, P. Direct Electrochemistry of Redox Enzymes as a Tool for Mechanistic Studies. *Chem Rev* **108**, 2379–2438 (2008).
35. Chiu, J. & Hogg, P. J. Allosteric disulfides: Sophisticated molecular structures enabling flexible protein regulation. *Journal of Biological Chemistry* **294**, 2949–5908 (2019).
36. Hartmann, T. & Leimkühler, S. The oxygen-tolerant and NAD⁺-dependent formate dehydrogenase from *Rhodobacter capsulatus* is able to catalyze the reduction of CO₂ to formate. *FEBS Journal* **280**, 6083–6096 (2013).
37. Yu, X., Niks, D., Mulchandani, A. & Hille, R. Efficient reduction of CO₂ by the molybdenum-containing formate dehydrogenase from *Cupriavidus necator* (*Ralstonia eutropha*). *Journal of Biological Chemistry* jbc.M117.785576 (2017). doi:10.1074/jbc.M117.785576
38. Graham, J. E., Niks, D., Zane, G. M., Gui, Q., Hom, K., Hille, R., Judy, D. & Raman, C. S. How a Formate Dehydrogenase Responds to Oxygen : Unexpected O₂ Insensitivity of an Enzyme Harboring Tungstate , Selenocysteine , and [4Fe-4S] Clusters. *ACS Catal* 1–55 (2022). doi:doi/10.1021/acscatal.2c00316
39. Hogg, P. J. Disulfide bonds as switches for protein function. *Trends Biochem Sci* **28**, 210–214 (2003).
40. Marie Wensien, Fabian Rabe von Pappenheim, Lisa-Marie Funk, Patrick Kloskowski, Ute Curth, Ulf Diederichsen, Jon Uranga, Jin Ye, Pan Fang, Kuan-Ting Pan, Henning Urlaub, Ricardo A. Mata, Viktor Sautner, K. T. A lysine-cysteine redox switch with an NOS bridge regulates enzyme function. *Nature* (2021). doi:10.1038/s41586-021-03513-3

41. Rabe von Pappenheim, F., Wensien, M., Ye, J., Uranga, J., Irisarri, I., de Vries, J., Funk, L.-M., Mata, R. A. & Tittmann, K. Widespread occurrence of covalent lysine–cysteine redox switches in proteins. *Nat Chem Biol* (2022). doi:10.1038/s41589-021-00966-5
42. Schrapers, P., Hartmann, T., Kositzki, R., Dau, H., Reschke, S., Schulzke, C., Leimkühler, S. & Haumann, M. Sulfido and cysteine ligation changes at the molybdenum cofactor during substrate conversion by formate dehydrogenase (fdh) from rhodobacter capsulatus. *Inorg Chem* **54**, 3260–3271 (2015).
43. Hakopian, S., Niks, D. & Hille, R. The air-inactivation of formate dehydrogenase FdsDABG from *Cupriavidus necator*. *J Inorg Biochem* 111788 (2022). doi:10.1016/j.jinorgbio.2022.111788
44. Agne, M., Appel, L., Seelmann, C. & Boll, M. Enoyl-Coenzyme A Respiration via Formate Cycling in Syntrophic Bacteria. *mBio* **13**, 1–16 (2022).
45. Schink, B., Montag, D., Keller, A. & Müller, N. Hydrogen or formate: Alternative key players in methanogenic degradation. *Environ Microbiol Rep* **9**, 189–202 (2017).
46. Dong, G. & Ryde, U. Reaction mechanism of formate dehydrogenase studied by computational methods. *JBIC Journal of Biological Inorganic Chemistry* **1**, 3 (2018).
47. Cypionka, H. Oxygen respiration by *Desulfovibrio* species. *Annu Rev Microbiol* **54**, 827–848 (2000).
48. Dolla, A., Fournier, M. & Dermoun, Z. Oxygen defense in sulfate-reducing bacteria. *J Biotechnol* **126**, 87–100 (2006).
49. Mukhopadhyay, A., Redding, A. M., Joachimiak, M. P., Arkin, A. P., Borglin, S. E., Dehal, P. S., Chakraborty, R., Geller, J. T., Hazen, T. C., He, Q., Joyner, D. C., Martin, V. J. J., Wall, J. D., Zamin, K. Y., Zhou, J. & Keasling, J. D. Cell-wide responses to low-oxygen exposure in *Desulfovibrio vulgaris* Hildenborough. *J Bacteriol* **189**, 5996–6010 (2007).
50. Fareleira, P., Santos, B. S., António, C., Moradas-Ferreira, P., LeGall, J., Xavier, A. V. & Santos, H. Response of a strict anaerobe to oxygen: Survival strategies in *Desulfovibrio gigas*. *Microbiology (N Y)* **149**, 1513–1522 (2003).
51. Imlay, J. A., Sethu, R. & Rohaun, S. K. Evolutionary adaptations that enable enzymes to tolerate oxidative stress. *Free Radic Biol Med* **140**, 4–13 (2019).
52. Lu, Z. & Imlay, J. A. When anaerobes encounter oxygen: mechanisms of oxygen toxicity, tolerance and defence. *Nat Rev Microbiol* **0123456789**, (2021).
53. Baumgarten, A., Redenius, I., Kranczoch, J. & Cypionka, H. Periplasmic oxygen reduction by *Desulfovibrio* species. *Arch Microbiol* **176**, 306–309 (2001).
54. Ramel, F., Amrani, A., Pieulle, L., Lamrabet, O., Voordouw, G., Company, M., Dolla, A., Brasseur, G., Seddiki, N. & Bre, D. Membrane-bound oxygen reductases of the anaerobic sulfate-reducing *Desulfovibrio vulgaris* Hildenborough: roles in oxygen defence and electron link with periplasmic hydrogen oxidation. 2663–2673 (2013). doi:10.1099/mic.0.071282-0

- 545 55. Fournier, M., Aubert, C., Dermoun, Z., Durand, M., Moinier, D. & Dolla, A. Response of the anaerobe
546 *Desulfovibrio vulgaris* Hildenborough to oxidative conditions : proteome and transcript analysis. **88**, 85–
547 94 (2006).
- 548 56. Vita, N., Hatchikian, E. C., Nouailler, M., Dolla, A. & Pieulle, L. Disulfide bond-dependent mechanism of
549 protection against oxidative stress in pyruvate-ferredoxin oxidoreductase of anaerobic *Desulfovibrio*
550 bacteria. *Biochemistry* **47**, 957–964 (2008).
- 551 57. Rodríguez-Maciá, P., Reijerse, E. J., van Gastel, M., DeBeer, S., Lubitz, W., Rüdiger, O. & Birrell, J. A.
552 Sulfide Protects [FeFe] Hydrogenases From O₂. *J Am Chem Soc* jacs.8b04339 (2018).
553 doi:10.1021/jacs.8b04339
- 554 58. Marques, M. C., Coelho, R., De Lacey, A. L., Pereira, I. A. C. & Matias, P. M. The three-dimensional
555 structure of [nifese] hydrogenase from *desulfovibrio vulgaris* hildenborough: A hydrogenase without a
556 bridging ligand in the active site in its oxidised, ‘as-isolated’ state. *J Mol Biol* **396**, 893–907 (2010).
- 557 59. Felbek, C., Arrigoni, F., de Sancho, D., Jacq-Bailly, A., Best, R. B., Fourmond, V., Bertini, L. & Léger, C.
558 Mechanism of Hydrogen Sulfide-Dependent Inhibition of FeFe Hydrogenase. *ACS Catal* **11**, 15162–
559 15176 (2021).
- 560 60. Wittenborn, E. C., Guendon, C., Merrouch, M., Benvenuti, M., Fourmond, V., Léger, C., Drennan, C. L. &
561 Dementin, S. The Solvent-Exposed Fe–S D-Cluster Contributes to Oxygen-Resistance in *Desulfovibrio*
562 *vulgaris* Ni–Fe Carbon Monoxide Dehydrogenase. *ACS Catal* **10**, 7328–7335 (2020).
563
564

Methods

Site-Directed Mutagenesis, Expression, and Protein Purification. FdhAB variants were produced by site-directed mutagenesis of *fdhA* gene in the pRec-FdhAB-Strep expression plasmid¹⁴ using the NZYMutagenesis kit. The primers used are presented in Supplementary Table 5. Correct mutations were confirmed by sequencing by Eurofins Genomic, Germany. Plasmid incorporation was performed by electroporation and cells were grown as reported for the *D. vulgaris* H $\Delta fdhAB$ deletion strain^{14,20,61}. For aerobic purification of FdhAB and its variants, the crude soluble extract was oxidized in air until the redox potential was stable (from an average of -270 mV to +155 mV, vs SHE). The affinity purification was performed following the protocol reported in¹⁴. For anaerobic purifications, all the purification steps were employed using N₂-flushed buffers. The disruption was equally done using the French pressure cell, and for that, a tube was adapted at the exit of the cell to connect with a rubber stopper closed glass shot through a needle. This way, a close circuit was created minimizing contact with air. After ultracentrifugation, the soluble fraction was flushed with N₂ to remove the remaining sulfide and 2 mM DTT was added. Affinity purification was performed inside a COY Anaerobic chamber with an atmosphere of 2% H₂/98% N₂. Unless otherwise stated, FdhAB was aerobically purified, while C872A and M405A were typically anaerobically purified. The buffer of eluted samples was exchanged to aerobic or anaerobic 20 mM Tris-HCl pH 7.6, 10% (v/v) glycerol and 10 mM NaNO₃ (Buffer A). Protein concentration was determined based on $\epsilon_{410nm} = 43.45 \text{ mM}^{-1}\text{cm}^{-1}$ ¹⁴. Purity of samples was judged by 12% SDS-polyacrylamide gel.

Solution Activity Assays. Routine solution enzymatic assays were done as previously reported¹⁴, with and without DTT pre-treatment, using a UV-1800 Shimadzu spectrophotometer, inside a COY Anaerobic chamber with an atmosphere of 2% H₂/98% N₂. A final concentration of 1.4 nM of enzyme was used for WT, C872A and C845A FdhAB variants, while for M405A a final concentration of 14 nM was used.

The effect of dithionite on enzyme activation was evaluated by incubating WT FdhAB for 5 minutes with 15 mM dithionite, corresponding to 100-fold relative to the enzyme. Excess dithionite was washed away using anaerobic buffer A and a 50- kDa cut-off centrifugal filter unit, and enzyme concentration was determined again, and the same 1.4 nM FdhAB were used in the activity assays, with and without DTT pre-treatment. Similarly, for the pre-activation with DTT, FdhAB was incubated for 5 minutes with 50 mM DTT, and the excess was removed as described above. The influence of pH on FDH activity was evaluated using a buffer mix of glycine, K₂HPO₄, citric acid and Tris, 25 mM each. The pH was adjusted using HCl or KOH.

For the determination of the affinity constants for formate, the activity of pure enzyme samples was measured at substrate concentrations ranging from 0.5 μM to 20 mM sodium formate, in 50 mM KPi buffer at the optimum pH of 7.6. In the case of affinity to CO₂, 125 μM to 50 mM of sodium bicarbonate were used, in 100 mM KPi at pH 7.1. The bicarbonate stock solutions (in 100 mM KPi, pH 7.1) were kept in fully filled flasks and the enzymatic reactions were carried out with a phase of mineral oil on top of the solution, to avoid headspace and minimise CO₂ loss to the gas phase. This revealed a lower K_M for CO₂ for the WT FdhAB than previously determined¹⁴. The pH of the enzymatic

reactions was confirmed for each point. CO₂ affinity of M405A was evaluated at pH 6. Activities with CO₂-saturated buffer were identical, as expected from the relatively fast CO₂-HCO₃⁻ equilibrium⁶².

Whole cell assays. *D. vulgaris* H cells expressing recombinant WT FdhAB were grown anaerobically, as previously reported¹⁴. The formate oxidation activity of fresh whole cells in growth medium (OD₆₀₀ = 0.3, 50 µl) was measured anaerobically, with and without 1 mM DTT in 1 ml of 50 mM KPi pH 7.6, 20 mM sodium formate, 15 mM ethylenediaminetetraacetic acid (EDTA) and 1 mM methyl viologen. Activities with DTT involved a 2.5 min pre-activation with 50 mM DTT. Reduction of methyl viologen was followed spectrometrically at 578 nm ($\epsilon_{578\text{ nm}}(\text{MV}^+) = 9.7\text{ mM}^{-1}\text{ cm}^{-1}$). Cell cultures were then exposed to air bubbling for 7 min, with stirring. Part of the cultures was shifted to N₂ bubbling for 10 min, while the remaining cultured remained exposed to air bubbling. It was previously shown that such oxidative stress induces a stress response, but does not lead to generalised cell death^{63–66}. Aliquots were periodically collected and evaluated for formate oxidation activity with and without DTT activation, as described for the initial activity. The *D. vulgaris* H ΔfdhAB deletion strain grown with tungsten showed no activity for formate oxidation, due to the low expression of the other two FDHs present in the genome¹⁹.

Thermal Shift Assays. The melting temperature of C872A and C845A was determined using the Applied Biosystems Protein Shift Dye Kit: 2 mg/mL of pure samples in buffer A were mixed with the dye (2-fold) and the melting curve recorded from 25 to 99°C, on the QuantStudio 7 Flex Real-time PCR system from Applied Biosystems.

Electrochemical Methods. All procedures were performed inside a Jacomex glove box with an atmosphere of N₂ (O₂ < 4 ppm). Aerobically isolated FdhAB was pre-treated with DTT by mixing 1 µL of 74 µM enzyme with 1 µL of 10 mM DTT, for 10 minutes. The mixture was diluted to 7.4 µM using buffer E (100 mM NaCl, 5 mM MES, 5 mM CHES, 5 mM HEPES, 5 mM TAPS, 5mM sodium acetate, pH 7.0). Anaerobically purified WT FdhAB, and C872A and C845A variants were not treated with DTT and were similarly diluted with buffer E. To produce the electroactive films the different enzyme preparations were co-absorbed on pyrolytic graphite edge rotating disc working electrode (PGE-RDE, 2.5 mm diameter), with polymyxin B sulfate (Sigma-Aldrich). For that 0.5 µL of 6 mg/mL polymyxin were deposited in PGE-RDE and left to dry, and then 0.5 µL of 7.4 µM enzyme solution were added and the electrode was used immediately before the enzyme solution dried, as described in⁶². The electrochemical measurements were performed in a standard three-electrode cell, a platinum wire was used as the counter electrode, and saturated calomel electrode as the reference electrode. Measurements were made using the Autolab PGSTAT128N potentiostat (Metrohm, The Netherlands) with the software GPES. The rotation of the working electrode to around 4000 rpm was controlled using an Autolab RDE 2 electrode rotator (Metrohm, The Netherlands). Chronoamperometric measurements were done in the presence of 1 mM formate in buffer E, and the potential poised to $E = 0.142\text{ V}$ vs standard hydrogen electrode (SHE). Additions of 30

632 $\mu\text{M O}_2$ were performed by injecting in the cell 50 μL of O_2 -saturated H_2O . The data was analyzed using the open-source
633 program QSoas⁶⁷ applying the following commands:
634 apply-formula $y=\log(y)$
635 filter-fft /derive=1
636 fit-exponential-decay
637 QSoas⁶⁷ is a free software available at <https://bip.cnrs.fr/groups/bip06/software/>
638

639 **EPR Spectroscopy.** The reduction of C872A variant (39 μM) prepared in 50 mM MOPS pH 7.6, 10% (v/v) glycerol was
640 done inside a glove box (Jacomex), at room temperature. The redox potential was measured in the titration cell with
641 a combined Pt-Ag/AgCl/KCl (3M) microelectrode. Methylene blue, indigo disulfonate, phenosafranine, methyl red, and
642 methyl viologen were used as mediators to a final concentration of 10 μM . Successive additions of either sodium
643 formate or sodium dithionite were done. After potential stabilization, a sample was collected to an EPR tube and
644 frozen immediately in the glove box. For the M405A variant, the reduction was performed inside the glove box by
645 adding directly a small volume of sodium formate or sodium dithionite to the EPR tubes.

646 EPR analysis was done on a Bruker ELEXSYS E500 spectrometer equipped with an ER41002ST standard
647 rectangular Bruker EPR cavity fitted to an Oxford Instruments ESR 900 helium flow cryostat. Double integration of EPR
648 spectra recorded in non-saturating conditions was done for spin intensity measurements, comparing with 1 mM
649 Cu(II)EDTA standard. EPR spectrum simulations were performed with EasySpin.
650

651 **Crystallization, Data Collection, Structure Solution, and Refinement.**

652 The crystal structures reported in this work were obtained from C872A samples purified anaerobically and
653 M405A purified in the presence of oxygen¹⁴. All crystals were obtained at 20°C using hanging-drop vapor diffusion
654 method, drops of 2 μL (1:1, protein:precipitant ratio) in 24 well plates (24 well XRL plate Molecular Dimensions). The
655 concentration of variant C872A was 18.2 mg/mL and the crystals appeared in three different conditions; C872A_ox
656 (aerobic conditions): 20 % PEG 3350 (w/v), 0.1 M Tris-HCl pH 8.5 and 0.2 M CaCl_2 (crystals appeared within 2 days);
657 C872A_anox* (anaerobic conditions): cocrystallized with 10 mM of azide in 22% PEG 3350 (w/v), 0.1 M Tris-HCl pH 8.5
658 and 0.2 M CaCl_2 (crystals appeared within 2 days); C872A_anox (anaerobic conditions): 32% PEG 3350, 0.1 M Tris HCl
659 pH 8.0, 1 M LiCl (the condition previously optimized for the wild type crystals¹⁴) with 0.2 μL of a dilution 1:100 from a
660 stock of microseeds from FdhAB wild type, these crystals were finally soaked for 30 min with 10 mM of sodium
661 formamide (crystals appeared within 30 days). All the anaerobic experiments were performed in an anaerobic
662 chamber under an argon atmosphere at <0.1 ppm of oxygen, and all the solutions were previously degassed and stored
663 in the anerobic chamber. Crystals of M405A (at 11.5 mg/mL) were obtained in 30% PEG 3350, 0.1 M Tris HCl pH 8.0

and 1 M LiCl in aerobic conditions. All crystals were transferred into a cryoprotectant solution consisting of the precipitant solution supplemented with 20% (v/v) glycerol, and then flash cooled in liquid nitrogen.

X-ray diffraction experiments were performed on ALBA (XALOC beamline)⁶⁸ and ESRF (ID23-1, ID30A-3 and ID30B)^{69–71} synchrotrons and the data were processed with the programs XDS⁷² and Aimless⁷³ or autoPROC⁷⁴ and STARANISO⁷⁵. The structures were solved by molecular replacement with Phaser⁷⁶ from the CCP4 suite⁷⁷, using as search model the previously published as-isolated structure (PDB ID: 6SDR) to the C872A_{ox} and M405A variants, C872A_{ox} for the C872A_{anox}*, and C872A_{anox}* for the C872A_{anox}. The models were refined with iterative cycles of manual model building with Coot⁷⁸ and refinement with REFMAC5⁷⁹. Data processing and refinement statistics are presented in Supplementary Table 1.

Sequence analysis. The amino acid sequence of *D. vulgaris* H FdhA (Uniprot Q72EJ1, Locus tag DVU0587, NCBI Reference Sequence: WP_010937890.1) was used as query in the Protein-Protein Basic Local Alignment Search Tool (BLASTp), against the RefSeq Selected proteins database (Feb 2021). Multiple sequence alignment was performed using Clustal Omega⁸⁰ and analyzed using Jalview software⁸¹ and *D. vulgaris* H FdhA as reference. The alignment was manually curated namely in the adjacent regions to positions 845 and 872.

The genome of bacteria identified as having a CC-FDH were selected on Integrated Microbial Genomes & Microbiomes (IMG/M), but only 77 from the 85 were available. A blast using DVU0587 as query was performed against the selected genomes and the locus tag of the respective FDH sequences containing the conserved cysteines (CC-FDH) were identified. Then the CC-FDH operons were analyzed to identify the complexity of FDH composition, named as AB for dimeric protein (catalytic and electron transfer subunit), ABC for trimeric protein containing an additional cytochrome *c*₃ subunit and ABG for trimeric protein containing a membrane-bound cytochrome *b* (λ subunit). The presence of a Tat signal peptide was predicted using SignalP - 5.0 software⁸².

Data availability

The data that support the findings of this study is available within the main text and its Supplementary Information file. Source data is provided as Source Data files. The atomic coordinates and structure factors for the *D. vulgaris* H C872A variant structures have been deposited in the Protein Data Bank under accession codes [8CM4](#), [8CM5](#), [8CM6](#) and [8CM7](#).

Methods-only references

61. Keller, K. L., Wall, J. D. & Chhabra, S. in *Synthetic Biology, Part A* **497**, 503–517 (Elsevier Inc., 2011).
62. Meneghello, M., Oliveira, A. R., Jacq-Bailly, A., Pereira, I. A. C., Léger, C. & Fourmond, V. Formate Dehydrogenases Reduce CO₂ Rather than HCO₃⁻: An Electrochemical Demonstration. *Angewandte Chemie International Edition* **60**, 9964–9967 (2021).
63. Cypionka, H. Oxygen respiration by *Desulfovibrio* species. *Annu Rev Microbiol* **54**, 827–848 (2000).

699 64. Dolla, A., Fournier, M. & Dermoun, Z. Oxygen defense in sulfate-reducing bacteria. *J Biotechnol* **126**, 87–100
700 (2006).

701 65. Mukhopadhyay, A., Redding, A. M., Joachimiak, M. P., Arkin, A. P., Borglin, S. E., Dehal, P. S., Chakraborty, R.,
702 Geller, J. T., Hazen, T. C., He, Q., Joyner, D. C., Martin, V. J. J., Wall, J. D., Zamin, K. Y., Zhou, J. & Keasling, J. D.
703 Cell-wide responses to low-oxygen exposure in *Desulfovibrio vulgaris* Hildenborough. *J Bacteriol* **189**, 5996–
704 6010 (2007).

705 66. Fareleira, P., Santos, B. S., António, C., Moradas-Ferreira, P., LeGall, J., Xavier, A. V. & Santos, H. Response of a
706 strict anaerobe to oxygen: Survival strategies in *Desulfovibrio gigas*. *Microbiology (N Y)* **149**, 1513–1522 (2003).

707 67. Fourmond, V. QSoas: A Versatile Software for Data Analysis. *Anal Chem* **88**, 5050–5052 (2016).

708 68. Juanhuix, J., Gil-Ortiz, F., Cuní, G., Colldelram, C., Nicolás, J., Lidón, J., Boter, E., Ruget, C., Ferrer, S. & Benach,
709 J. Developments in optics and performance at BL13-XALOC, the macromolecular crystallography beamline at
710 the Alba Synchrotron. *J Synchrotron Radiat* **21**, 679–689 (2014).

711 69. McCarthy, A. A., Barrett, R., Beteva, A., Caserotto, H., Dobias, F., Felisaz, F., Giraud, T., Guijarro, M., Janocha,
712 R., Khadrouche, A., Lentini, M., Leonard, G. A., Lopez Marrero, M., Malbet-Monaco, S., McSweeney, S., Nurizzo,
713 D., Papp, G., Rossi, C., Sinoir, J., Sorez, C., Surr, J., Svensson, O., Zander, U., Cipriani, F., Theveneau, P. &
714 Mueller-Dieckmann, C. ID30B – a versatile beamline for macromolecular crystallography experiments at the
715 ESRF. *J Synchrotron Radiat* **25**, 1249–1260 (2018).

716 70. Nurizzo, D., Mairs, T., Guijarro, M., Rey, V., Meyer, J., Fajardo, P., Chavanne, J., Biasci, J. C., McSweeney, S. &
717 Mitchell, E. The ID23-1 structural biology beamline at the ESRF. *J Synchrotron Radiat* **13**, 227–238 (2006).

718 71. Von Stetten, D., Carpentier, P., Flot, D., Beteva, A., Caserotto, H., Dobias, F., Guijarro, M., Giraud, T., Lentini,
719 M., McSweeney, S., Royant, A., Petitdemange, S., Sinoir, J., Surr, J., Svensson, O., Theveneau, P., Leonard, G.
720 A. & Mueller-Dieckmann, C. ID30A-3 (MASSIF-3) - A beamline for macromolecular crystallography at the ESRF
721 with a small intense beam. *J Synchrotron Radiat* **27**, 844–851 (2020).

722 72. Kabsch, W. XDS. *Acta Crystallogr D Biol Crystallogr* **66**, 125–132 (2010).

723 73. Evans, P. R. & Murshudov, G. N. How good are my data and what is the resolution? *Acta Crystallogr D Biol*
724 *Crystallogr* **69**, 1204–1214 (2013).

725 74. Vonrhein, C., Flensburg, C., Keller, P., Sharff, A., Smart, O., Paciorek, W., Womack, T. & Bricogne, G. Data
726 processing and analysis with the autoPROC toolbox. *Acta Crystallogr D Biol Crystallogr* **67**, 293–302 (2011).

727 75. Vonrhein, C., Tickle, I. J., Flensburg, C., Keller, P., Paciorek, W., Sharff, A. & Bricogne, G. Advances in automated
728 data analysis and processing within autoPROC, combined with improved characterisation, mitigation and
729 visualisation of the anisotropy of diffraction limits using STARANISO. *Acta Cryst. A Found Adv.* **74**, 43537 (2018).

730 76. McCoy, A. J., Grosse-Kunstleve, R. W., Adams, P. D., Winn, M. D., Storoni, L. C. & Read, R. J. Phaser
731 crystallographic software. *J Appl Crystallogr* **40**, 658–674 (2007).

732 77. Winn, M. D., Ballard, C. C., Cowtan, K. D., Dodson, E. J., Emsley, P., Evans, P. R., Keegan, R. M., Krissinel,
733 E. B., Leslie, A. G. W., McCoy, A., McNicholas, S. J., Murshudov, G. N., Pannu, N. S., Potterton, E. A., Powell, H.

- R., Read, R. J., Vagin, A. & Wilson, K. S. Overview of the CCP4 suite and current developments. *Acta Crystallogr D Biol Crystallogr* **67**, 235–242 (2011).
78. Emsley, P., Lohkamp, B., Scott, W. G. & Cowtan, K. Features and development of Coot. *Acta Crystallogr D Biol Crystallogr* **66**, 486–501 (2010).
79. Murshudov, G. N., Skubák, P., Lebedev, A. A., Pannu, N. S., Steiner, R. A., Nicholls, R. A., Winn, M. D., Long, F. & Vagin, A. A. REFMAC5 for the refinement of macromolecular crystal structures. *Acta Crystallogr D Biol Crystallogr* **67**, 355–367 (2011).
80. Sievers, F. & Higgins, D. G. Clustal Omega for making accurate alignments of many protein sequences. *Protein Science* **27**, 135–145 (2018).
81. Waterhouse, A. M., Procter, J. B., Martin, D. M. A., Clamp, M. & Barton, G. J. Jalview Version 2-A multiple sequence alignment editor and analysis workbench. *Bioinformatics* **25**, 1189–1191 (2009).
82. Savojardo, C., Martelli, P. L., Fariselli, P. & Casadio, R. DeepSig: Deep learning improves signal peptide detection in proteins. *Bioinformatics* **34**, 1690–1696 (2018).

Figure 1

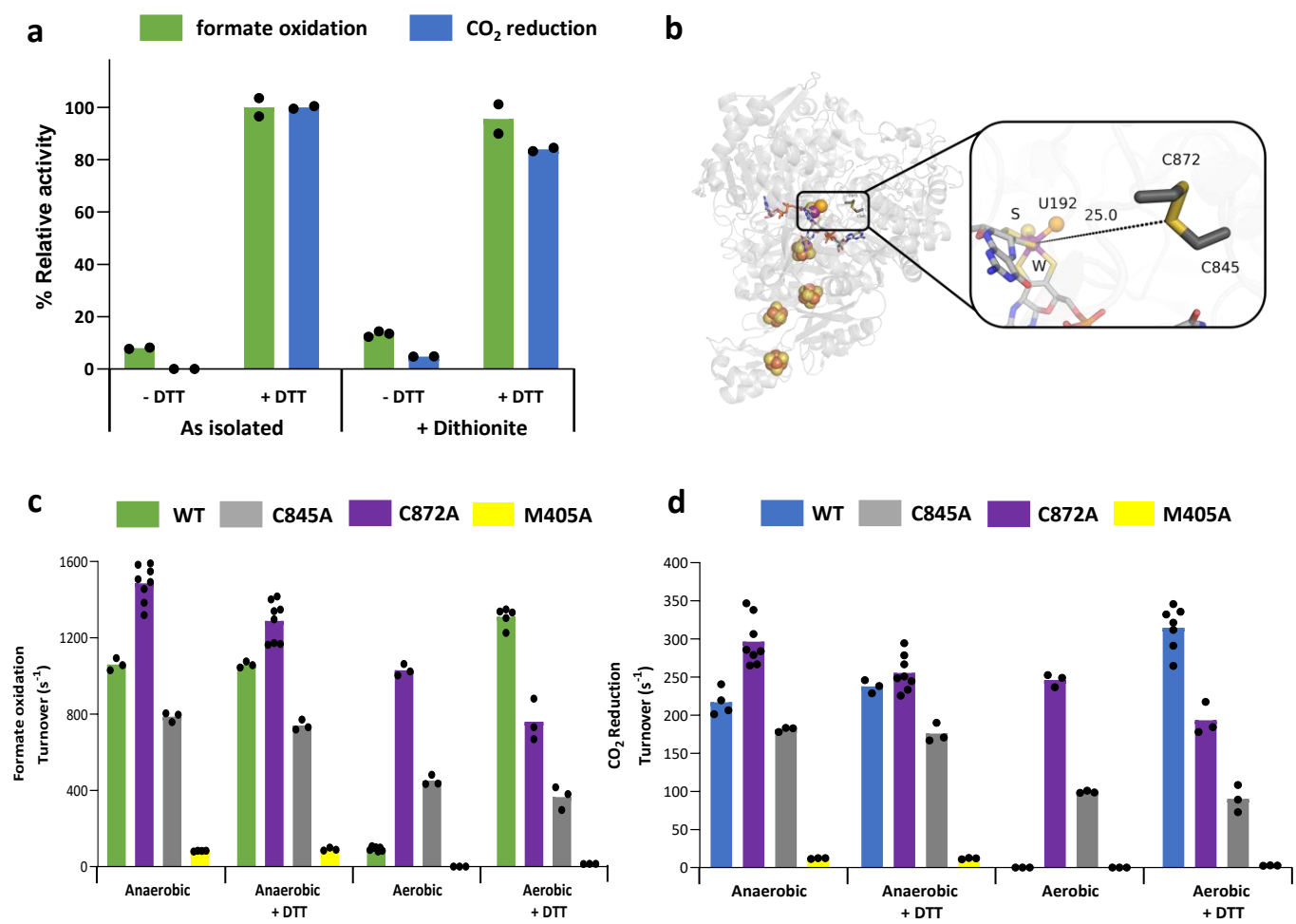


Figure 2

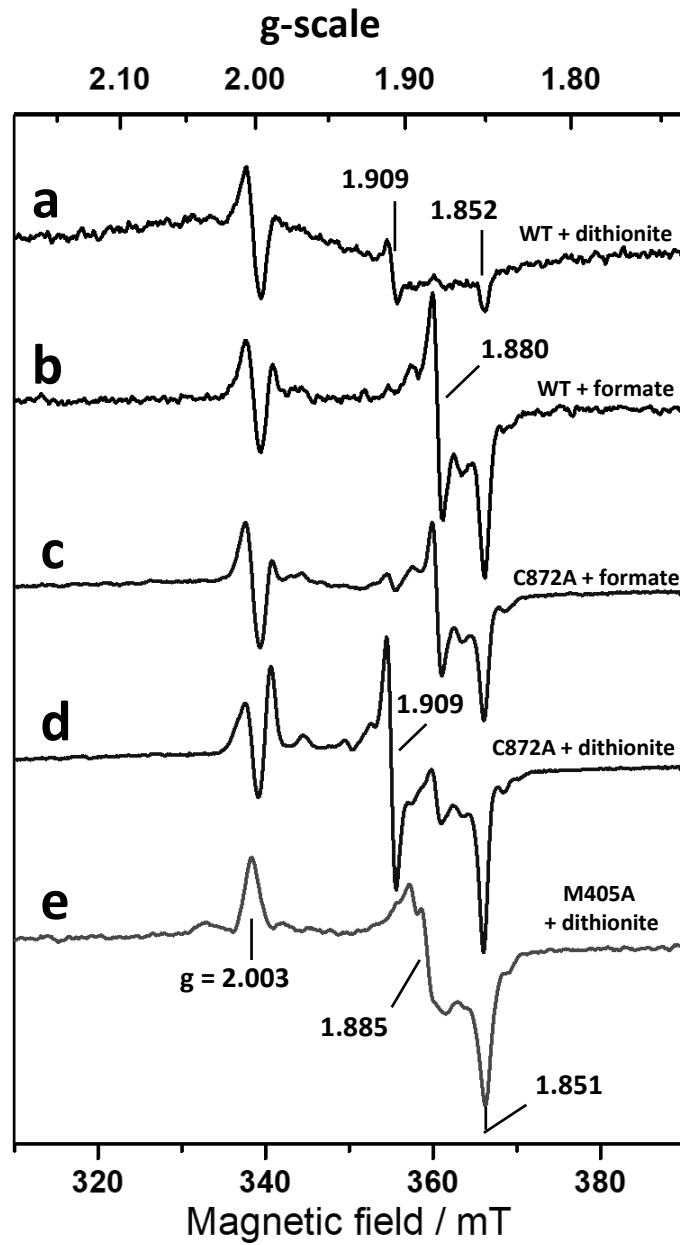


Figure 3

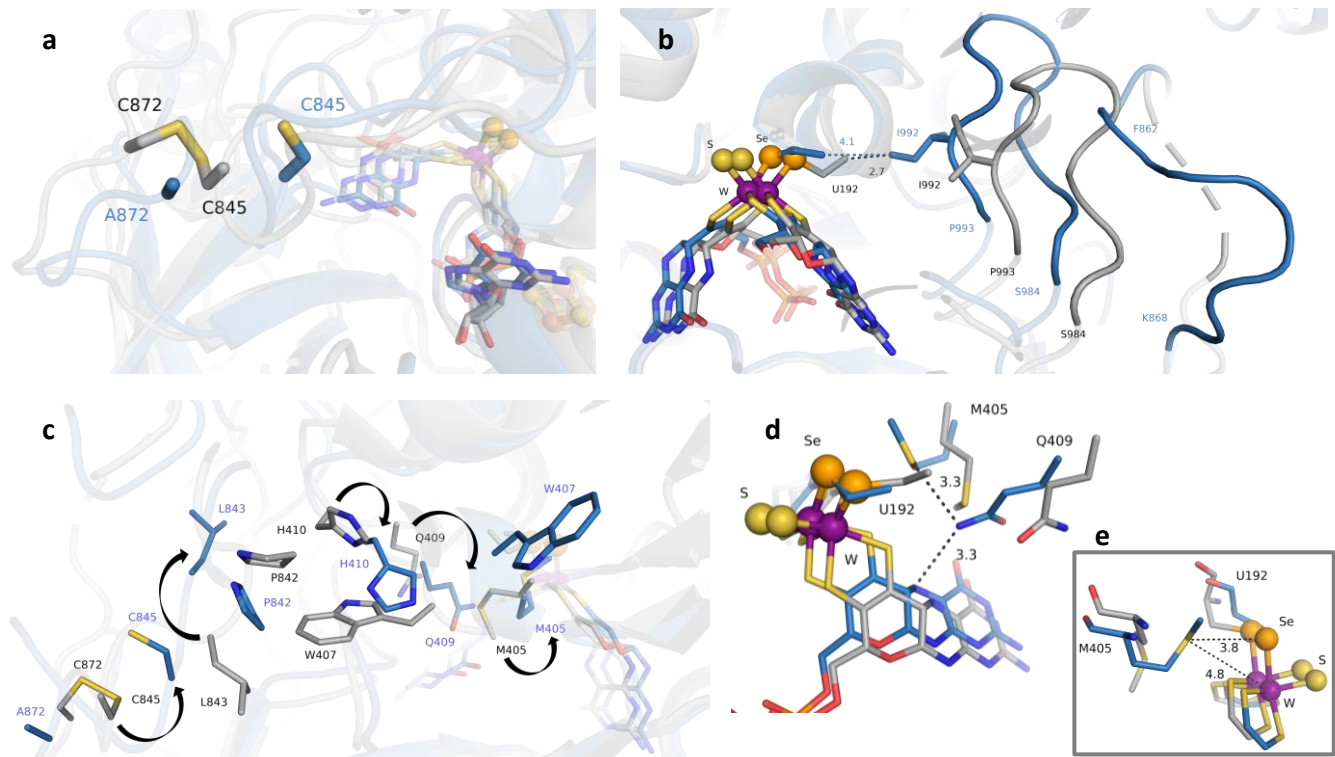


Figure 4

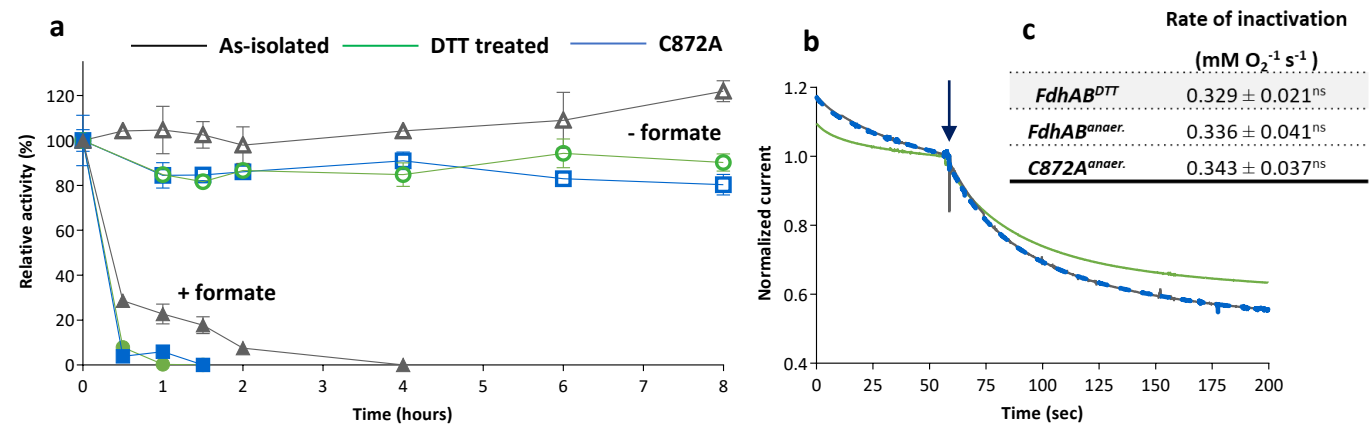


Figure 5

